

DEEP NEURAL NETWORK APPROXIMATIONS FOR THE STABLE MANIFOLDS OF THE HAMILTON-JACOBI-BELLMAN EQUATIONS

GUOYUAN CHEN

ABSTRACT. For an infinite-horizon control problem, the optimal control can be represented by the stable manifold of the characteristic Hamiltonian system of Hamilton-Jacobi-Bellman (HJB) equation in a semiglobal domain. In this paper, we first theoretically prove that if an approximation is sufficiently close to the exact stable manifold of the HJB equation in a certain sense, then the control derived from this approximation stabilizes the system and is nearly optimal. Then, based on the theoretical result, we propose a deep learning algorithm to approximate the stable manifold and compute optimal feedback control numerically. The algorithm relies on adaptive data generation through finding trajectories randomly within the stable manifold. Such kind of algorithm is grid-free basically, making it potentially applicable to a wide range of high-dimensional nonlinear systems. We demonstrate the effectiveness of our method through two examples: stabilizing the Reaction Wheel Pendulums and controlling the parabolic Allen-Cahn equation.

1. INTRODUCTION

It is well known that solving Hamilton-Jacobi-Bellman (HJB) equation is essentially complicated in general and requires advanced computation tools and techniques. In this paper, we focus on the stationary HJB equations which are related to infinite-horizon optimal control and H^∞ control problems. The stabilizing solutions of the stationary HJB equations correspond to the stable manifolds of the characteristic Hamiltonian systems at equilibriums (cf. e.g. [36, 38]). Once the stable manifold is obtained, the optimal control can be represented directly by it, without using the gradient of the solution of the HJB equation ([36]). This approach can be viewed as an extension of LQ theory to nonlinear systems.

Computing stable manifolds for Hamilton-Jacobi (HJ) equations is generally a challenging task. In [36], the authors introduced an iterative procedure aimed at approximating the precise trajectories of the characteristic Hamiltonian system on the stable manifold. While this method has demonstrated effectiveness in generating effective feedback controls for specific initial conditions or near nominal trajectories, as demonstrated in [5, 15, 16, 35], it can become time-consuming when applied to computing feedback controls for more general initial states or for high-dimensional state systems.

Numerous studies have been dedicated to numerically solving various HJ equations. See e.g. [1, 3, 10, 18, 20, 26, 29]. However, as pointed out in [27], these existing methods may encounter several limitations, including heavy computational costs for high-dimensional systems, challenges in estimating solution accuracy for general systems, solutions being limited to a small neighborhood of a fixed point or

nominal trajectory, and the necessity for special structures in the nonlinear terms of the system.

In recent years, various deep learning methods have emerged for efficiently solving HJ equations in large high-dimensional domains using grid-free sampling. For example, [37] suggests utilizing neural networks (NN) to approximate solutions of the HJ equation by minimizing the residual of the PDEs and boundary conditions on a set of randomly sampled collocation points. [13] and [32] introduce deep learning method for solving PDEs, including HJB equations, by reformulating the PDEs as stochastic differential equations. [25] establishes a theory for employing NN to approximate optimal feedback laws on appropriate functional spaces. [27] and [21] propose a causality-free data-driven deep learning algorithm for solving HJB equations, enhancing the effectiveness of NN training through adaptive data generation. Interested readers can refer to [12] for a comprehensive review of this direction.

The aim of this paper is to seek semiglobal deep NN approximations of stable manifolds. The main contributions are as follows. Firstly, we theoretically prove that, given appropriate accuracy assumptions, the control derived from the NN approximation of the stable manifold stabilizes the system and is sufficiently close to the exact optimal control (Theorem 3.2 in Section 3). Secondly, based on the theoretical results, we propose an algorithm for finding deep NN approximations of stable manifolds. One of the crucial aspects of this algorithm is a composite loss function that incorporates the maximum error, the mean error of the NN from the exact stable manifold on the sample set, and the error between the derivative of the NN at the origin and the stabilizing solution of the Riccati equation (as shown in equation (4.1) below). Another crucial issue is adaptive data generation by solving the characteristic Hamiltonian systems which is inspired by [27]. Specifically, we solve two-point boundary value problems (BVPs) locally near the equilibrium and extend the local solutions using initial value problems (IVPs) for the characteristic Hamiltonian system. We randomly choose a number of samples along each trajectory, and adaptively select additional samples near points with large errors from the previous round of training. Our approach is causality-free and does not depend on discretizing the space, making it suitable for high-dimensional problems. Causality-free algorithms have been successful in various applications. See e.g. [7, 13, 22–24, 39].

Our approach differs from those focused on solving the HJB equations, e.g., [27, 37]. Our method is based on the stable manifold, an intrinsic geometric property of the HJB equation. With this framework, we can ensure the stability of the closed loop from the controller generated by the trained NN satisfying certain accuracy. There are few theoretical results on this topic in the literature. In empirical algorithms, the ‘equilibrium’ of the closed loop system from the NN may become unstable or disappear as time goes to infinity, as shown in [28]. Moreover, our method is different from that in [28], which devises certain architectures for approximate NN to stabilize the system. It is worth noting that in [5, 35, 36], the algorithms are based on an iterative procedure in a small neighborhood of the equilibrium, which is difficult to estimate the accuracy and is time-consuming to generate trajectories.

To demonstrate the effectiveness of our method, we present two applications: stabilizing the Reaction Wheel Pendulum (RWP) and optimal control of the parabolic Allen-Cahn (AC) equation. The NN training for both problems is performed

on an ordinary laptop, demonstrating the practicality and efficiency of our approach. In particular, by simulation, the time to generate the control signal from the trained NN takes less than one millisecond on average. This implies that our method enables real-time control in practice.

The paper is structured as follows. Section 2 gives an overview of stable manifold method. Section 3 presents theoretical results. Section 4 outlines the deep learning algorithm. Sections 5 and 6 give the examples. Appendix A includes proof of Theorem 3.2.

2. THE STABLE MANIFOLDS OF THE HJB EQUATIONS

In this section, we outline some basic results about the stable manifolds of the HJB equations from nonlinear control theory. Although the stable manifold method can be applied to problems that are nonlinear in control, to emphasize our main point clearly, we focus on control-affine systems

$$\dot{x} = f(x) + g(x)u, \quad \text{in } \Omega, \quad (2.1)$$

where g is Lipschitz continuous $n \times m$ matrix-valued function, u is an m -dimensional feedback control, $\Omega \subset \mathbb{R}^n$ is a bounded domain with piecewise smooth boundary containing 0. Let the instantaneous cost be $L(x, u) = q(x) + \frac{1}{2}u^T W u$, where $W > 0$ is an $m \times m$ symmetric matrix, $q(x)$ is a smooth nonnegative function. Define the cost functional by $J(x, u) = \int_0^{+\infty} L(x(t), u(t))dt$. The corresponding HJB equation is

$$\nabla V^T(x)f(x) - 1/2\nabla V^T(x)R\nabla V(x) + q(x) = 0. \quad (2.2)$$

Here $\nabla V = (\frac{\partial V}{\partial x_1}, \dots, \frac{\partial V}{\partial x_n})^T$ is the gradient of the value function V , and

$$R(x) := g(x)W^{-1}g(x)^T.$$

The corresponding feedback control function $u(x) = -W^{-1}g(x)^T\nabla V(x)$. Plugging it into (2.1), we obtain the closed-loop system

$$\dot{x} = f(x) - R(x)\nabla V(x), \quad \text{in } \Omega. \quad (2.3)$$

Throughout the paper, the following assumption will be made:

- (C₁) Assume that $f(x)$ and $q(x)$ are C^∞ in Ω . For $|x|$ small, $f(x) = Ax + O(|x|^2)$ and $q(x) = \frac{1}{2}x^T Q x + O(|x|^3)$ with $A \in \mathbb{R}^{n \times n}$, and $Q \in \mathbb{R}^{n \times n}$ is symmetric. Function $g : \Omega \rightarrow \mathbb{R}^{n \times m}$ is C^∞ .

Recall that a solution V of (2.2) is said to be the *stabilizing solution* if $\nabla V(0) = 0$ and 0 is an asymptotically stable equilibrium of (2.3). The characteristic Hamiltonian system of (2.2) is

$$\begin{cases} \dot{x} = f(x) - R(x)p \\ \dot{p} = -(\frac{\partial f(x)}{\partial x})^T p + \frac{1}{2} \frac{\partial(p^T R(x)p)^T}{\partial x} - (\frac{\partial q}{\partial x})^T. \end{cases} \quad (2.4)$$

Assume V is a stabilizing solution of (2.2), let $\Lambda_V := \{(x, p) \mid p = \nabla V(x)\}$. Then Λ_V is invariant under the flow (2.4) (see e.g. [38]). Note that 0 is an equilibrium of (2.4) and the Hamiltonian matrix at 0 is $\text{Ham} = \begin{pmatrix} A & -R(0) \\ -Q & -A^T \end{pmatrix}$. We assume the following condition:

(C_2) Ham is hyperbolic and the generalized eigenspace E_- for n -stable eigenvalues satisfies the complementary condition $E_- \oplus \text{Im}(0, I_n)^T = \mathbb{R}^{2n}$, where I_n is the identity matrix of dimension n .

Then the following result for stable manifolds holds ([38]).

Theorem 2.1. *Assume that f, q, R satisfy conditions ($C_1 - C_2$). Then the stable manifold of (2.4) through $(x, p) = (0, 0)$ is a smooth submanifold of dimension n in \mathbb{R}^{2n} . Moreover, in a neighborhood of $(0, 0)$, this submanifold is the graph Λ_V . In particular, there exist $\delta > 0$ and $k > 0$ such that for all $|x| < \delta$, $|p(x) - Px| \leq k|x|^2$, where $P = \frac{\partial^2 V}{\partial x^2}(0)$.*

Recall that P is also the stabilizing solution of the Riccati equation ([38])

$$PA + A^T P - PR(0)P + Q = 0, \quad (2.5)$$

which can be considered as quadratic approximation of the HJB equation (2.2) at 0.

Remark 2.1. *From Theorem 2.1, the stabilizing solution V of (2.2) is C^∞ in a neighborhood of 0 in \mathbb{R}^n . In this paper, we assume that V is a C^2 function, and the graph representation of the stable manifold, Λ_V , is semiglobal, meaning that it holds in a properly large domain Ω containing the origin. It is challenging to determine the exact domain where the graph representation holds due to its close relationship with the regularity of V . Specifically, if V is not differentiable at x_0 , then the graph representation may not hold at x_0 (cf [4]).*

To find trajectories of (2.4), we solve a two-point BVP in a small neighborhood of the origin. Specifically, following [36], we set $\mathcal{T} = \begin{pmatrix} I & S \\ P & PS + I \end{pmatrix}$, and $\begin{pmatrix} \bar{x} \\ \bar{p} \end{pmatrix} = \mathcal{T}^{-1} \begin{pmatrix} x \\ p \end{pmatrix}$, where S is the solution of the Lyapunov equation $(A - R(0)P)S + S(A - R(0)P) = R(0)$. The system (2.4) becomes

$$\begin{cases} \dot{\bar{x}} = (A - R(0)P)\bar{x} + N_s(\bar{x}, \bar{p}) \\ \dot{\bar{p}} = -(A - R(0)P)^T \bar{p} + N_u(\bar{x}, \bar{p}). \end{cases} \quad (2.6)$$

Here $N_s(\bar{x}, \bar{p}), N_u(\bar{x}, \bar{p})$ are the nonlinear terms except the linear terms in (2.4). We solve (2.6) with boundary condition

$$\bar{x}(0) = \bar{x}_0, \quad \bar{p}(+\infty) = 0. \quad (2.7)$$

From [36, Theorem 5], we have

Proposition 2.1. *Suppose conditions (C_1)-(C_2) hold. For \bar{x}_0 sufficiently small, there exists unique trajectory of the two-point BVP (2.6)-(2.7) contained in the stable manifold near 0.*

3. ASYMPTOTIC ANALYSIS OF APPROXIMATE CLOSED-LOOP SYSTEM

This section provides an asymptotic analysis of the closed-loop system based on approximations of the stable manifold. Hereafter, we assume that f, q , and R satisfy conditions (C_1)-(C_2), and that V is the stabilizing solution of (2.2). In this paper, we use certain deep NN $p^{NN}(\theta, \cdot)$ to approximate $p(x) = \nabla V(x)$. The universal approximation theorem for NN guarantees that there exists NN approximation $p^{NN}(\theta, \cdot)$ that is sufficiently close to $p(x)$ if the number of parameters θ of the NN

is large enough (see [17], [31]). The details of the NN will be presented in Section 4 below. Recall that the exact optimal control is given by

$$u(x) = -W^{-1}g(x)^T p(x). \quad (3.1)$$

Subsequently, the approximation of the optimal control is

$$u^{NN}(x) = -W^{-1}g(x)^T p^{NN}(\theta, x). \quad (3.2)$$

Assume that $x(t)$ is the solution of

$$\dot{x} = f(x) - R(x)p(x), \quad x(0) = x_0, \quad (3.3)$$

$x^{NN}(t)$ is the solution of the approximate closed-loop system

$$\dot{x} = f(x) - R(x)p^{NN}(\theta, x), \quad x(0) = x_0. \quad (3.4)$$

From Condition (C_1) , it holds that there exist constants $b > 0$ and $k > 0$ such that for all $|x| < b$,

$$\begin{aligned} |f(x) - Ax| &< k|x|^2, & |g(x) - g(0)| &< k|x|, \\ |R(x) - R(0)| &< k|x|. \end{aligned} \quad (3.5)$$

Since f, g, R are C^∞ in Ω , we have that f, g, R are Lipschitz continuous in any compact subset of Ω . Moreover, Remark 2.1 yields that p is Lipschitz continuous in Ω . Hereafter, without loss of generality, the Lipschitz constant of f, g, R, p can be chosen as a unified constant L .

Theorem 3.1. *Let $x(t)$ be the solution of (3.3). There exist constants $C > 0$, $b > 0$, $\alpha > 0$ such that $|x(t)| \leq C|x_0|e^{-\alpha t}$, for $t \geq 0$ and $|x_0| \leq b$.*

Proof. From Theorem 2.1 and (3.5), there exist $k_0 > 0$ and $b > 0$ such that $|f(x) - R(x)p(x) - (Ax - R(0)Px)| \leq k_0|x|^2$, for all $|x| < b$. Since all eigenvalues of $A - R(0)P$ has negative real part, the result holds from [6, Theorem 2.77]. \square

Remark 3.1. *Let $B = A - R(0)P$. There exists a constant $\beta > 0$ such that $|e^{Bt}x_0| \leq |x_0|e^{-\beta t}$. Hence $\alpha \rightarrow \beta^-$ as $b \rightarrow 0$ in Theorem 3.1.*

Corollary 3.1. *Let $\Psi \subset \Omega$ be any compact set. For any $\varepsilon > 0$, by Theorem 3.1, there exists a constant $T_\varepsilon > 0$ such that $|x(t)| < \varepsilon/2$, $\forall t \geq T_\varepsilon$, for all $x_0 \in \Psi$. We call T_ε an admissible time of x with respect to ε .*

Proof. From Theorem 3.1 and Remark 2.1, it holds that for any $x_0 \in \Psi$, there exists $T_{\varepsilon, x_0} > 0$ depending on ε and x_0 such that $|x(t)| < \varepsilon/2$, $\forall t \geq T_{\varepsilon, x_0}$. Furthermore, using the continuous dependence of solutions on initial data of ODE and the compactness of Ψ , we have the existence of uniform constant $T_\varepsilon > 0$ independent on x_0 such that $|x(t)| < \varepsilon/2$, $\forall t \geq T_\varepsilon$. \square

For $x^{NN}(t)$, we have the following asymptotic result whose proof will be included in Appendix below.

Theorem 3.2. *Let P be the stabilizing solution of the Riccati equation (2.5), let $\gamma_0 > 0$ be a fixed constant, and let $\Psi \subset \Omega$ be any compact set. For any $\varepsilon \in (0, \gamma_0)$, there exist $\delta > 0$ and $\eta > 0$ such that if $p^{NN}(\theta, \cdot)$ satisfies the following conditions: (a) $|p^{NN}(\theta, x) - p(x)| < \delta$ for all $x \in \Omega$; (b) $|p^{NN}(\theta, x) - Px| \leq \eta|x|$ for $|x| < \gamma_0$, then, $|x^{NN}(t) - x(t)| < \varepsilon$ for all $t > 0$, and $x^{NN}(t)$ (resp. $x(t)$) decays exponentially as $t \rightarrow +\infty$. Here, $x^{NN}(t)$ is the solution of (3.4) (resp. the solution of (3.3)) with arbitrary $x_0 \in \Psi$. Consequently, $|J(x^{NN}, u^{NN}) - J(x, u)| < C\varepsilon$ where C is a constant depending only on f, g, R, p, W .*

4. ALGORITHM

In this section, we propose a deep learning algorithm based on the theoretical result in Theorem 3.2 to find $p^{NN}(\theta, \cdot)$ that is sufficiently close to $p(\cdot)$ in the sense of conditions (a)-(b) in Theorem 3.2.

4.1. Architecture of the NN. To achieve certain accuracy, the number of parameters of the NN depends essentially on its architecture. For example, the complexity of deep compositional networks utilizing standard ReLUs for approximating Lipschitz continuous functions with a given accuracy depends linearly on the dimension n . See e.g. [31, Theorem 4]. In contrast, the complexity required by an NN with only one hidden layer to achieve a similar level of accuracy grows exponentially with the dimension n . This phenomenon is known as the curse of dimensionality for the complexity of the NN. See e.g. [31, Theorem 1]. In this paper, rather than delving further into the architecture of the NN, we *empirically* use a deep NN of LSTM type with smooth activation function $\sin(\cdot)$ (see e.g. [14], [37]). However, we should emphasize that other types of deep NN may also work well. As in [27, 30, 37], to mitigate the curse of dimensionality, we focus the investigation on control aspect and develop the algorithm based on gridfree method.

In the following, we utilize an LSTM type NN, $p_o^{NN}(\theta; x)$, as in [37, Section 4.2]. Suppose input x and output p are n -dimensional, the number of hidden layers is l and each layer has m units. Different from [37, Section 4.2], we use $\sigma : \mathbb{R}^m \rightarrow \mathbb{R}^m$, $\sigma(z) = (\sin(z_1), \dots, \sin(z_m))$ as the activation function. The derivative of $\sin(\cdot)$, namely $\cos(\cdot)$, has more global support than the derivatives of the traditional activation functions such as sigmoid. Moreover, we modify the original NN by $p^{NN}(\theta, x) = p_o^{NN}(\theta, x) - p_o^{NN}(\theta, 0)$. Then $p^{NN}(\theta, 0) = 0$, which is a necessary condition for p^{NN} to satisfy condition (b) in Theorem 3.2.

To fit our theoretical conclusion in Section 3, we define the loss function as follows: for $\nu \in [1, \infty]$,

$$\begin{aligned} \mathcal{L}^\nu(\theta; \mathcal{D}) := & \sigma_1 \left[\frac{1}{|\mathcal{D}|} \sum_{i=1}^{|\mathcal{D}|} \|p_i - p^{NN}(\theta; x_i)\|^\nu \right] \\ & + \sigma_2 \max_{p_i \in \mathcal{D}} |p_i - p^{NN}(\theta; x_i)| + \sigma_3 \left\| \frac{\partial p^{NN}}{\partial x}(\theta, 0) - P \right\|, \end{aligned} \quad (4.1)$$

where $|\cdot|$ denotes the standard Euclidean norm in \mathbb{R}^n , $\|\cdot\|$ is the operator norm of the matrix, $|\mathcal{D}|$ is the number of samples in \mathcal{D} , and $\sigma_i > 0$ for $i = 1, 2, 3$ are weight constants. The first term measures the mean error with exponent ν between the NN predicted value $p^{NN}(\theta; x_i)$ and the standard value p_i on dataset \mathcal{D} ; the second term enforces that the maximum difference between the predicted and observed values is small; and the third term ensures that the derivative of the NN function at 0 is close to the stabilizing solution P of the Riccati equation (2.5). The weight constants σ_i control the relative importance of these terms in the overall loss function.

4.2. The algorithm. Inspired by [27], we propose a deep learning algorithm based on adaptive data generation on the stable manifold. The sketch of the algorithm is as follows.

Step 0. Transformation of the model. We begin by rescaling the characteristic Hamiltonian system (2.4). The necessity of such a transformation is explained in Subsection 4.3.5 below.

Step 1. First generation of trajectories and sampling. We find a certain number of trajectories on the stable manifold by solving two-point BVP near the equilibrium and extending the local trajectories by IVP as described in Subsection 4.3.1 below. Then we pick out some samples on each trajectory to obtain a training set $\mathcal{D}_1 := \{(x_i, p_i)\}_{i=1}^{N_1}$ as in Subsection 4.3.2 below. Similarly, we also generate a set of samples, \mathcal{D}^{val} , for validation of the trained NN later.

Step 2. First NN training. We train an LSTM type NN, $p^{NN}(\theta, \cdot)$, with parameters θ , on \mathcal{D}_1 satisfying $p^{NN}(\theta, x_i) \approx p_i$, $i = 1, \dots, N_1$, for some epochs. If $p^{NN}(\theta, \cdot)$ satisfies $\mathcal{L}^\nu(\theta, \mathcal{D}_1) < \varepsilon$ for empirically chosen ε , then we check $p^{NN}(\theta, \cdot)$ on \mathcal{D}^{val} to obtain the test error.

Step 3. Adaptive data generation. If the test error is not good enough, then we generate more samples near the points with relatively large errors from the first round training. Adding these new samples to \mathcal{D}_1 , we obtain a larger sample set \mathcal{D}_2 . For details see Subsection 4.3.3 below.

Step 4. Model refinement. Based on the NN obtained in Step 2, we continue training the NN on the updated data set \mathcal{D}_2 as in Step 2. The training procedure stops once the NN satisfies a Monte Carlo test as in Subsection 4.3.4 below.

Step 5. Approximate optimal feedback control. From $p^{NN}(\theta, \cdot)$, we can get the approximate optimal feedback control u^{NN} (3.2) and compute the closed-loop trajectories at certain initial conditions $x(0) = x_0$ by solving (3.4).

Remark 4.1. *To enhance the performance and to prove the convergence of the procedure in the sense of mean square error (MSE) while minimizing computational costs, we can utilize a sample size selection scheme based on the sample variances of the training sets \mathcal{D}_i , $i = 1, 2, \dots$, following the approach proposed in [27, Section 4.1].*

4.3. Key techniques of the algorithm. As mentioned above, our approach is to find NN approximation of the stable manifold, which differs from the method in [27]. Moreover, to improve the effectiveness of our algorithm, we incorporate several useful techniques as follows.

4.3.1. Generating trajectories by two-point BVP and IVP. We first use ‘scipy.integrate.solve_bvp’ to solve the two-point BVP (2.6)-(2.7) for $x_0 \in \partial B_r(0)$, where $r > 0$ is small, and $\partial B_r(0)$ denotes the sphere centered at 0 with radius r . This BVP solver implements a 4th-order collocation method with control of residuals (see [19]). The BVP solver requires an initial mesh for time and an initial guess for the solution values at each mesh node. The iterative procedure of the solver may diverge if the initial guess is not well chosen. For problem (2.6)-(2.7), the boundary condition x_0 are chosen on a small ball $\partial B_r(0)$, and the initial guess is constantly 0 at each mesh node. To select an appropriate radius r , we employ a Monte Carlo method. Specifically, we first choose a small r , randomly take some points on the ball $\partial B_r(0)$, then solve (2.6)-(2.7). If the success rate of the BVP solver is 100%, then we choose a slightly larger r . This procedure continues until the success rate of the BVP solver is not 100%.

We then extend the local solutions, $(\tilde{x}(t), \tilde{p}(t))$, $t \geq 0$, obtained by the BVP solver. On some interval $(T_-, 0]$, $T_- < 0$, we solve the following IVP:

$$\begin{cases} \dot{x} = f(x) - R(x)p, \\ \dot{p} = -\left(\frac{\partial f(x)}{\partial x}\right)^T p + \frac{1}{2} \frac{\partial(p^T R(x)p)^T}{\partial x} - \left(\frac{\partial q}{\partial x}\right)^T, \end{cases} \quad \text{with } x(0) = \tilde{x}(0), p(0) = \tilde{p}(0). \quad (4.2)$$

To solve this IVP, we can use ‘scipy.integrate.solve_ivp’ with various methods (e.g., ‘RK45’, ‘Radau’, etc.), as well as symplectic methods, variational integrators. Comparing to the BVP solver, the IVP (4.2) is usually much easier to solve. To approximate T_- , we first choose a value $T_-^0 < 0$ and check whether the IVP solver successfully computes the solution for all initial conditions $(\tilde{x}(0), \tilde{p}(0))$ on $(T_-^0, 0]$. If the success rate is 100%, we then choose a slightly smaller value $T_-^1 < T_-^0 < 0$, and repeat the procedure until the IVP solver fails at some initial conditions.

4.3.2. Sampling along trajectories. Since Theorem 3.1 and Remark 3.1 yield that the decay of the trajectory $x(t)$ is almost $e^{-\beta t}$ as $t \rightarrow +\infty$, we empirically select samples on the trajectories near the origin according to an exponential distribution $\rho(t) = \frac{1}{\lambda} e^{-\frac{t}{\lambda}}$ for $t > 0$ with $\lambda = \beta_{\min}^{-1}$. Here β_{\min} is the distance between the set of eigenvalues and the imaginary axis. That is, if we take t_0, t_1, t_2, \dots from the exponential distribution, then $(x(t_0), p(t_0)), (x(t_1), p(t_1)), (x(t_2), p(t_2)), \dots$ lie on the stable manifold. Moreover, we select a certain number of samples on $(T_-, 0]$ according to uniform distribution.

4.3.3. Adaptive data generation. After the first round training, we record the absolute errors of $p^{NN}(\theta, \cdot)$ on \mathcal{D}_1 as $|p^{NN}(\theta, x_i) - p_i|$, $i = 1, \dots, N_1$. We then select the largest $[\mu N_1]$ points on \mathcal{D}_1 , where $[y]$ is the integer part of y and $\mu \in (0, 1)$ is chosen as in [27, Section 4.1]. Denote the set of these samples by $\hat{\mathcal{D}}_1$. We randomly sample J_1 points $y_j \in \Omega$ ($j = 1, \dots, J_1$) around x_i with $(x_i, p_i) \in \hat{\mathcal{D}}_1$ according to some Gaussian distribution, then find solutions of (2.6)-(2.7) with $x(0) = y_j$ by BVP solver. Here, the initial guess of the solution is the trajectory, $(x_i(t), p_i(t))$, $t \in (T_-, \infty)$, where (x_i, p_i) lies on. We choose L_1 samples on each new trajectory according to a certain Gaussian distribution for $t > 0$. Adding these new samples in \mathcal{D}_1 , we obtain a larger sample set \mathcal{D}_2 .

4.3.4. Monte Carlo test of the NN. To obtain the error bounds as in Theorem 3.2, we use a Monte Carlo test. Specifically, we randomly select a certain number of initial points according to uniform distribution in Ω . Using the trained NN, $p^{NN}(\theta, \cdot)$, we generate feedback control u^{NN} as (3.2), then check if the closed-loop trajectories is stabilized at these initial points by solving (3.4). If the trained NN works well, then the test error gives the error bounds in Theorem 3.2.

4.3.5. Rescaling. For concrete applications, the original formulation of models may not be suitable for numerical methods. Hence, modifications, such as coordinate transformations, should be made at the beginning of the algorithm. In our algorithm, we use rescaling, which also appears in computational optimal control (see, e.g., [33, 34]). In (2.4), we apply a rescaling $(\hat{x}_1, \hat{x}_2, \dots, \hat{x}_n) = (\lambda_1 \bar{x}_1, \lambda_2 \bar{x}_2, \dots, \lambda_n \bar{x}_n)$ so that the variables $(\hat{x}_1, \hat{x}_2, \dots, \hat{x}_n)$ (and their derivatives) have the same orders of magnitude. There are two advantages of rescaling. Firstly, after rescaling, the proportion of convergent rate by the BVP solver increases. As mentioned, we set constant on mesh nodes as initial guess of the solution in ‘scipy.integrate.solve_bvp’.

Hence if the value and derivative of the exact solution are too large, then the BVP solver may diverge. Secondly, rescaling enhances the effectiveness of NN training. The loss function (4.1) indicates that when the magnitudes of x_1, x_2, \dots, x_n differ significantly, certain variables in (4.1) may carry more weight, while others may have relatively smaller weights and could potentially be negligible. Figure 4 in Section 5 below shows essence of the rescaling.

5. APPLICATION TO THE REACTION WHEEL PENDULUMS

The RWP is a mechanical system that consists of a physical pendulum with a rotating disk (see Figure 1). Researchers have been interested in the swing up and stabilization of various pendulums for the past two decades (see, e.g., [2, 16, 35]).

The ideal dynamical system of the RWP is given by $\dot{x}_1 = x_2$, $\dot{x}_2 = a \sin x_1 - b_p u$, $\dot{x}_3 = b_r u$. Here u is an input function, $x_1 = \theta$, $x_2 = \dot{\theta}$, $x_3 = \dot{\theta}_r$. we borrow the parameters of instrument in [2, Page 21]: $a = 78.4$, $b_p = 1.08$, $b_r = 198$. Define a rescaling by $x_1 = \lambda_1 \bar{x}_1$, $x_2 = \lambda_2 \bar{x}_2$, $x_3 = \lambda_3 \bar{x}_3$. Then the system becomes $\dot{\bar{x}}_1 = \frac{\lambda_2}{\lambda_1} \bar{x}_2$, $\dot{\bar{x}}_2 = \frac{a}{\lambda_2} \sin(\lambda_1 \bar{x}_1) - \frac{b_p}{\lambda_2} u$, $\dot{\bar{x}}_3 = \frac{b_r}{\lambda_3} u$. Let $k = \frac{\lambda_2}{\lambda_1} = \sqrt{a}$ and $\sigma = \frac{b_p}{\lambda_2} = \frac{b_r}{\lambda_3}$. We choose $\lambda_1 = 1$ since we are mainly concerned with $x_1 \in [-\pi, \pi]$. Then $\lambda_2 = \sqrt{a}$ and $\lambda_3 = \frac{b_r}{b_p} \lambda_2$. With a little abuse of notations, we still use (x_1, x_2, x_3) instead of $(\bar{x}_1, \bar{x}_2, \bar{x}_3)$ for simplicity. Then $k = \lambda_2 \approx 8.85$, $\lambda_3 \approx 1623.30$, $\sigma = \frac{b_p}{\lambda_2} \approx 0.12$. Letting $x = (x_1, x_2, x_3)^T$, $f(x) = (kx_2, k \sin x_1, 0)^T$, $g(x) = (0, -\sigma, \sigma)^T$, the system has form (2.1). Define the instantaneous cost as $L(x, u) = \frac{1}{2}(x^T x + 0.01u^2)$. We implement an LSTM type NN, $p^{NN}(\theta, \cdot)$, in PyTorch with $l = 3$ and $m = 50$.

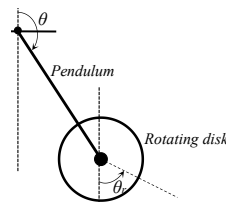


Figure 1: The Reaction Wheel Pendulum

We train the NN as the algorithm in Section 4.2.

1) *First sampling, training and validation*: Set the error tolerance of ‘scipy.integrate.solve_bvp’ to be 10^{-7} . The infinite interval $[0, +\infty)$ can be replaced by $[0, 20]$ to achieve numerical accuracy (since $\beta_{\min} = 1.2$). The initial mesh of t is $0, h, \dots, 100h$, with $h = 0.2$, and the initial guess of the solution is 0 at all these nodes. We randomly select 200 points $x_i \in \partial B_{0.5}(0)$ according to the uniform distribution. With these points as boundary conditions x_0 for the BVP solver, we solve (2.6)-(2.7) successfully. Next, we solve the IVP (4.2) using ‘scipy.integrate.solve_ivp’ with ‘method=Radau’, ‘rtol= 10^{-5} ’ (relative tolerance), and ‘atol= 10^{-7} ’ (absolute tolerance). Monte Carlo test infers $T_- = -0.2$. Thus 200 trajectories are obtained on the stable manifold. Finally, we select 5 points in $[0, 20]$ obeying the exponential distribution with $\lambda = 0.83$, and choose 20 points on $[-0.2, 0]$ according to the uniform distribution. Then, we pick out the samples (x_i, p_i) such that $x_i \in \Omega := [-3.2, 3.2] \times [-3.2, 3.2] \times [-3.2, 3.2]$. The set of these samples is denoted by $\mathcal{D}_1^{\text{train}}$, with $|\mathcal{D}_1^{\text{train}}| = 4363$. Similarly, solving 50 trajectories on the stable manifold yields a validation set \mathcal{D}^{val} with size 1081.

We train the NN using the internal optimizer Adam in PyTorch with 6000 epochs and learning rate $lr = 0.001 \times 0.5^{\lfloor j/1000 \rfloor}$ where j is the epoch. Set $\nu = 1$, $\sigma_1 = 1.0$, $\sigma_2 = \sigma_3 = 0.01$ in (4.1). After this round of training, the loss (4.1) on $\mathcal{D}_1^{\text{train}}$ is 7.5×10^{-3} , and the test loss on \mathcal{D}^{val} is 1.09×10^{-2} . The running time of the training is about 250 seconds on a ThinkPad T480s laptop without GPU.

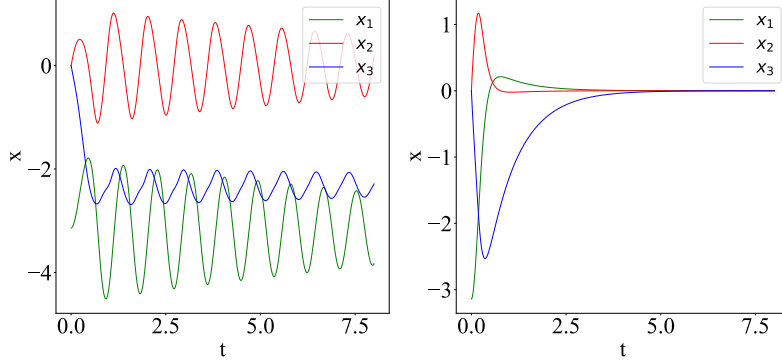


Figure 2: Simulations with initial states at hanging position based on first round training (left subfigure) and second round training (right subfigure).

2) *Adaptive sampling and refinement of the NN*: After the first round training, we find that the NN does not work well at some points, see e.g. Figure 2, by Monte Carlo test in Subsection 4.3.4. To improve the NN, we adaptively generate samples as in Subsection 4.3.3 with $\sigma = 0.1$, $J_1 = 5$ and $L_1 = 3$. Then we add the new samples in $\mathcal{D}_1^{\text{train}}$, obtaining updated training set $\mathcal{D}_2^{\text{train}}$ with a size of 10652. Based on the NN trained after the first round, we continue to train $p^{NN}(\theta, \cdot)$ on $\mathcal{D}_2^{\text{train}}$ for 6000 epochs with learning rate $lr = 2 \times 10^{-4} \times 0.5^{\lfloor j/1500 \rfloor}$, where j denotes the epoch. The training time is approximately 1000 seconds. Training loss on $\mathcal{D}_2^{\text{train}}$ is 7.3×10^{-3} , and the test loss is 9.3×10^{-3} . Monte Carlo test in Subsection 4.3.4 shows the NN works well.

3) *Simulations*: Numerical simulations are based on the NN generated feedback control (3.2). Figure 3 shows the closed-loop trajectories at some states from (3.4). Moreover, we compare the cost of the stable manifold (SM) method with the classical LQR and the optimal control obtained from the BVP solver. Table 1 shows the costs at several points. It is evident that the cost of the stable manifold method is much smaller than that of LQR and is very close to the optimal control obtained from the BVP solver when $|x_0|$ is relatively large, whereas the difference between the three costs is small when x_0 is near the origin. Note that here we obtain the optimal control by using $(x^{NN}(t), p^{NN}(t))$ generated by the NN as the initial guess to solve the BVP (2.6)-(2.7) successfully.

Table 1: Comparison of the costs at certain points

Initial positions	SM method	LQR	Optimal control
$(\pi, 0, 0)$	12.4	38.0	11.7
$(-0.8\pi, 0.1, 0.2)$	14.2	25.0	14.0
$(-0.6\pi, -0.2, -0.4)$	20.5	25.5	20.4
$(0.1\pi, 0, 0)$	0.8096	0.8115	0.8096
$(0.2, 0.03, -0.08)$	0.4055	0.4060	0.4055

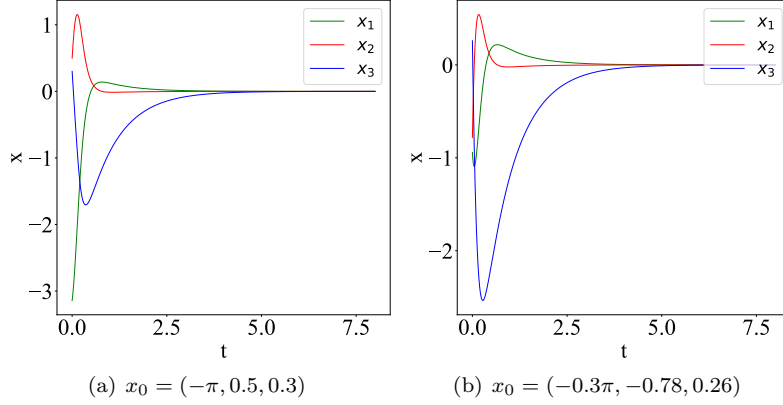


Figure 3: Closed-loop stabilizing trajectories of the Reaction Wheel Pendulum with some initial positions x_0 after the second round training.

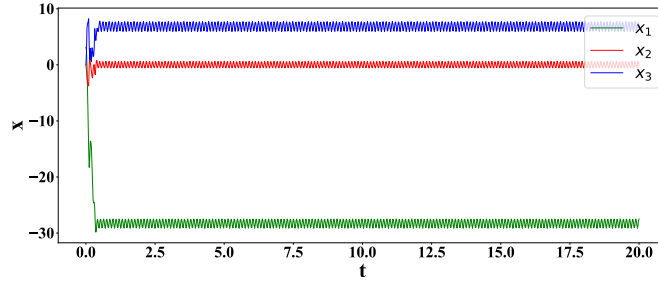


Figure 4: Sample closed-loop trajectory at $x_0 = (\pi, 0, 0)$ after the second round of training without rescaling at the beginning.

Additionally, Figure 4 shows that the system without rescaling at the beginning cannot generate good NN feedback controllers.

6. APPLICATION TO OPTIMAL CONTROL FOR THE PARABOLIC ALLEN-CAHN EQUATION

To illustrate the effectiveness of our algorithm for high-dimensional problems, we give an application to optimal control of the parabolic Allen-Cahn (AC) equation as follows,

$$\begin{aligned} \partial_t \mathcal{X}(\gamma, t) &= \sigma \partial_{\gamma\gamma} \mathcal{X}(\gamma, t) + \mathcal{X}(\gamma, t) - \mathcal{X}(\gamma, t)^3 + u, \\ &\text{in } \mathcal{I} \times \mathbb{R}^+, \end{aligned} \quad (6.1)$$

$$\mathcal{X}(-1, t) = 0, \quad \mathcal{X}(1, t) = 0, \quad t \in \mathbb{R}^+, \quad (6.2)$$

$$\mathcal{X}(\gamma, 0) = \mathcal{X}_0, \quad \gamma \in \mathcal{I}. \quad (6.3)$$

Here $\mathcal{I} = [-1, 1]$. The cost function is

$$J(u, \mathcal{X}_0) := \frac{1}{2} \int_0^\infty \left(\|\mathcal{X}(\cdot, t)\|_{L^2(\mathcal{I})}^2 + \|u(t)\|_{L^2(\mathcal{I})}^2 \right) dt.$$

The AC equation models a phase separation process ([11]). The optimal control of AC equation is a typical infinite dimensional control problem ([8, 9]). In this example, we approximate the AC equation by a high-dimensional system. Let N be an integer greater than 3, $h = \frac{2}{N}$ and $\gamma_i = -1 + \frac{2i}{N}$, $i = 0, 1, \dots, N$. Then $\mathcal{X}(\gamma_0, t) = \mathcal{X}(\gamma_N, t) = 0$, and for $i = 1, \dots, N-1$, $\mathcal{X}_{\gamma\gamma}(\gamma_i) \approx \frac{1}{h^2}(\mathcal{X}(\gamma_{i+1}) - 2\mathcal{X}(\gamma_i) + \mathcal{X}(\gamma_{i-1}))$. Let $X(t) = (X_1(t), \dots, X_{N-1}(t)) = (\mathcal{X}(\gamma_1, t), \dots, \mathcal{X}(\gamma_{N-1}, t))$. Define

$$A = \frac{1}{h^2} \begin{pmatrix} -2 & 1 & 0 & 0 & \cdots & 0 & 0 \\ 1 & -2 & 1 & 0 & \cdots & 0 & 0 \\ \vdots & \vdots & \vdots & \vdots & \vdots & \vdots & \vdots \\ 0 & 0 & 0 & 0 & \cdots & 1 & -2 \end{pmatrix}$$

Hence $\mathcal{X}_{\gamma\gamma} \approx AX$. Set $u = (u_1, u_2, \dots, u_{N-1})^T$. Then (6.1)-(6.3) becomes a discrete control system $\frac{d}{dt}X = f(X) + u$, where $X(0) = X_0 = (\mathcal{X}_0(\gamma_1), \dots, \mathcal{X}_0(\gamma_{N-1}))$, $f(X) = (\sigma A + I_{N-1})X - X^3$, $X^3 = (X_1^3, \dots, X_{N-1}^3)$. The cost function becomes $\int_0^\infty (\frac{1}{N}\|X(t)\|^2 + \frac{1}{N}\|u(t)\|^2) dt$, where $\|\cdot\|$ denotes the standard Euclid norm in \mathbb{R}^{N-1} . The HJB equation is

$$\nabla V^T(X)f(X) - \frac{1}{2}\nabla V^T(X)R\nabla V(X) + \frac{1}{N}X^T X = 0.$$

Here $R := \frac{N}{2}I_{N-1}$, where I_{N-1} is identity matrix of order $N-1$. The feedback control $u(X) = -\frac{N}{2}\nabla V(X)$. The Hamiltonian matrix at 0 is hyperbolic for $N > 3$.

In the numerical experiment, we choose $N = 31$. We utilize an LSTM type NN via PyTorch with $l = 3$ and $m = 60$. Let $\nu = 1$, $\sigma_1 = 1$ and $\sigma_2 = \sigma_3 = 0.1$ in the loss function (4.1). The error tolerance of `scipy.integrate.solve_bvp` is set to be 10^{-7} , $[0, +\infty)$ is replaced by $[0, 30]$ to ensure numerical accuracy since $\beta_{\min} = 1.021$. The initial mesh of t is $0, h, 2h, \dots, 100h$, with $h = 0.3$. We choose $B_{0.8}(0) \subset \mathbb{R}^{30}$ by Monte Carlo test, and select 1500 points x_i on the sphere $\partial B_{0.8}$ according to uniform distribution. Here the norm in \mathbb{R}^{30} is $|X| = \sqrt{\frac{1}{30} \sum_{i=1}^{30} X_i^2}$. The BVP solver with these settings successfully solves (2.6)-(2.7) for all 1500 boundary conditions. Next, we solve IVP (4.2) using the ‘`scipy.integrate.solve_ivp`’ with ‘`method=Radau`, `rtol=10-5` (relative tolerance), `atol=10-7` (absolute tolerance)’. A Monte Carlo test shows $T_- = -0.03$. Finally, we choose 23 points in $[0, 30]$ according the exponential distribution with $\lambda = 1$ and select 3 points according uniform distribution in $[-0.03, 0]$. This yields a total of 39000 samples, denoted by $\mathcal{D}_1^{\text{train}}$. Similarly, we generate a validation set \mathcal{D}^{val} by solving 200 trajectories on the stable manifold.

We use the internal optimizer Adam in PyTorch with a learning rate $lr = 0.01 \times 0.5^{\lfloor j/1500 \rfloor}$, where j is the iterative times, and train the NN for 6000 epochs. After training, we achieve the train loss on $\mathcal{D}_1^{\text{train}}$ being 1.3×10^{-3} and the test loss on \mathcal{D}^{val} being 1.6×10^{-3} . The training process takes approximately 5400 seconds on a ThinkPad T480s laptop without using GPU. Monte Carlo test as in Subsection 4.3.4 indicates that the trained NN works well. Figure 5 demonstrates the trajectories at two initial states.

Finally, we compare the cost of the NN-generated controller, the LQR, and the standard BVP solver. When the initial function is large, the cost of the NN-generated feedback controller is much smaller than that of the LQR, and is very close to that of the standard BVP solver. As in the previous example, we use

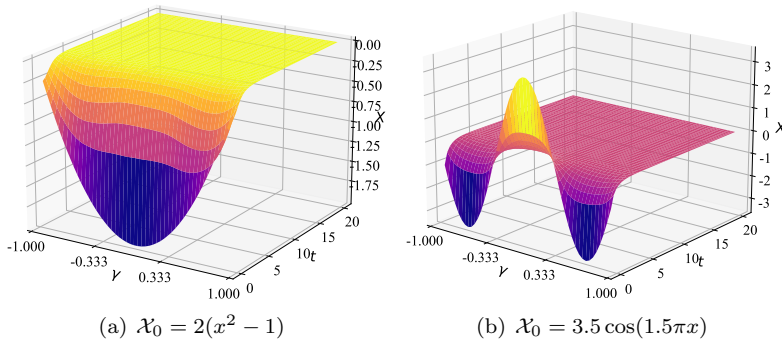


Figure 5: The dynamics of the NN controlled system at some initial states.

$(x^{NN}(t), p^{NN}(t))$ generated by the trained NN as the initial guess to solve the BVP (2.6)-(2.7).

Table 2: Comparison of the costs for certain initial states

Initial states	SM method	LQR	Optimal control
$3.5 \cos(1.5\pi x)$	1.91	3.36	1.86
$2(x^2 - 1)$	2.04	2.92	1.96
$2.5(x - 1)(x + 1)^3$	2.15	4.39	2.10
$0.3 \sin(\pi x)$	0.09673	0.09678	0.09667
$0.5(x - 1)(x + 1)^3$	0.0488	0.0513	0.0488

Remark 6.1. Each evaluation of our NN-generated control signal takes on average less than one millisecond (0.95×10^{-3} second) on a ThinkPad T480s laptop. This is faster than the controllers in [30] and [27], whose time to generate control signals is at least several milliseconds. This fast control signal generation time is crucial for real-time applications.

7. CONCLUSION

This paper proves that, under some natural conditions, NN approximations of the stable manifold of the HJB equation can generate nearly optimal controllers. Moreover, the approximate NN-controlled system is exponentially stable at the equilibrium as t tends to $+\infty$. Based on the theoretical conclusion, we propose an algorithm to construct a type of deep NN semiglobal approximations for the stable manifold. Our method relies on the geometric features of the HJB equations. The main advantage is that the derivatives of the value function of the optimal problem need not be calculated in the training procedure and computation of feedback control. The algorithm is based on adaptive data generation by finding trajectories on the stable manifold. Such kind of algorithm is grid-free, and is suitable for high-dimensional systems. The effectiveness of our framework is illustrated by stabilizing the Reaction Wheel Pendulum and seeking optimal control of the parabolic Allen-Cahn equation.

APPENDIX A. PROOF OF THEOREM 3.2

Proof of Theorem 3.2. Inspired by [6, Proof of Theorem 2.77], we give a proof which focuses on the perturbation feature of the system.

Recalling that $f(x) = Ax + O(|x|^2)$, $R(x) = R(0) + O(|x|)$, $p(x) = Px + O(|x|^2)$ and $B = A - R(0)P$, we rewrite (3.3) and (3.4) as

$$\dot{x} = Bx + (f(x) - Ax) - (R(x)p(x) - R(0)Px) := Bx + n(x), \quad x(0) = x_0,$$

and

$$\dot{x} = Bx + (f(x) - Ax) - (R(x)p^{NN}(\theta, x) - R(0)Px) := Bx + n^{NN}(x), \quad x(0) = x_0.$$

1. Note that

$$x(t) = e^{Bt}x_0 + \int_0^t e^{B(t-s)}n(x(s))ds$$

and

$$x^{NN}(t) = e^{Bt}x_0 + \int_0^t e^{B(t-s)}n^{NN}(x^{NN}(s))ds.$$

Then $x^{NN}(t) - x(t) = \int_0^t e^{B(t-s)}(n^{NN}(x^{NN}(s)) - n(x(s)))ds$. We first assume $x^{NN}(t) \in \Omega$. Hence $|R(x^{NN}(t))| < C$, $|p(x^{NN}(t))| < C$, $|R(x^{NN}(t)) - R(x(t))| \leq L|x^{NN}(t) - x(t)|$. From Condition (a) in Theorem 3.2, $|n^{NN}(x^{NN}(s)) - n(x(s))| \leq |f(x^{NN}(s)) - f(x(s))| + |R(x^{NN}(s))||p^{NN}(\theta, x^{NN}(s)) - p(x^{NN}(s))| + |p(x^{NN}(s))||R(x^{NN}(s)) - R(x(s))| + |R(x(s))||p(x^{NN}(s)) - p(x(s))| \leq CL|x^{NN}(s) - x(s)| + C\delta$. Using Remark 3.1 and setting $y(t) = |x^{NN}(t) - x(t)|$, it holds that

$$y(t) \leq C\beta^{-1}\delta + \int_0^t CLe^{-\beta(t-s)}y(s)ds. \quad (\text{A.1})$$

Hence

$$\frac{d}{dt} \log \left(C\beta^{-1}\delta + \int_0^t CLe^{-\beta(t-s)}y(s)ds \right) \leq CL.$$

Therefore

$$\log \left(C\beta^{-1}\delta + \int_0^t CLe^{-\beta(t-s)}y(s)ds \right) \leq \log(C\beta^{-1}\delta) + CLt.$$

By (A.1), $y(t) \leq C\beta^{-1}\delta e^{CLt}$. Using Corollary 3.1, it holds that for

$$\delta < C^{-1}\beta e^{-CLT_{\varepsilon_1}}\varepsilon_1/2,$$

$y(t) < \varepsilon_1/2$, $|x^{NN}(T_{\varepsilon_1})| < \varepsilon_1$, and, $x^{NN}(t) \in \Omega$ for all $t \in [0, T_{\varepsilon_1}]$, provided some $0 < \varepsilon_1 < \gamma_0$. Hence the assumption at the beginning of the proof is satisfied if $x(0) = x_0 \in \Psi$ and $\text{dist}(\partial\Psi, \partial\Omega) < \varepsilon_1$. Here $\text{dist}(\partial\Psi, \partial\Omega)$ denotes the distance between the boundaries of Ψ and Ω .

2. Let $\varepsilon \in (0, \gamma_0)$ be a constant sufficiently small, and let $\varepsilon_1 < \varepsilon$. Assume $I = \{t \geq T_{\varepsilon_1} \mid |x^{NN}(t)| < \varepsilon\}$. Moreover, we have

$$x^{NN}(t) = e^{Bt}x^{NN}(T_{\varepsilon_1}) + \int_{T_{\varepsilon_1}}^t e^{B(t-s)}n^{NN}(x^{NN}(s))ds.$$

For $t \in I$, since $|p^{NN}(\theta, x^{NN}(t)) - Px^{NN}(t)| \leq \eta|x^{NN}(t)|$ (Condition (b) in Theorem 3.2), it holds that

$$\begin{aligned}
& |n^{NN}(x^{NN}(t))| && \text{(A.2)} \\
& \leq |f(x^{NN}(t)) - Ax^{NN}(t)| + |(R(x^{NN}(t))p^{NN}(\theta, x^{NN}(t)) - R(0)Px^{NN}(t))| \\
& \leq k|x^{NN}(t)|^2 + |R(x^{NN}(t)) - R(0)||Px^{NN}(t)| \\
& \quad + |R(x^{NN}(t))||p^{NN}(\theta, x^{NN}(t)) - Px^{NN}(t)| \\
& \leq C_1((k+1)\varepsilon + \eta)|x^{NN}(t)|,
\end{aligned}$$

where C_1 is a constant depending only on f, R, p . It follows that

$$\begin{aligned}
|x^{NN}(t)| & \leq C|x^{NN}(T_{\varepsilon_1})|e^{-\beta(t-T_{\varepsilon_1})} && \text{(A.3)} \\
& + CC_1((k+1)\varepsilon + \eta) \int_{T_{\varepsilon_1}}^t e^{-\beta(t-s)}|x^{NN}(s)|ds.
\end{aligned}$$

Rewrite (A.3) as

$$|x^{NN}(t)|e^{\beta(t-T_{\varepsilon_1})} \leq C|x^{NN}(T_{\varepsilon_1})| + CC_1((k+1)\varepsilon + \eta) \int_{T_{\varepsilon_1}}^t e^{\beta(s-T_{\varepsilon_1})}|x^{NN}(s)|ds.$$

Using the Gronwall inequality (see e.g. [6, Theorem 2.1]), we find that

$$|x^{NN}(t)| \leq C|x^{NN}(T_{\varepsilon_1})|e^{-\alpha(t-T_{\varepsilon_1})}, \quad \text{(A.4)}$$

where $\alpha = \beta - CC_1((k+1)\varepsilon + \eta)$. If the two positive constants ε, η sufficiently small, then $\alpha > 0$. In the following, we assume that the constant C in (A.4) is greater than 2.

3. We prove that for $\varepsilon_1 < \varepsilon/C$, $I = [T_{\varepsilon_1}, \infty)$. If not, then there exists a $\bar{T} < \infty$ such that $I = [T_{\varepsilon_1}, \bar{T})$. Since $|x^{NN}(T_{\varepsilon_1})| < \varepsilon/C$, from (A.4) we get that $|x^{NN}(t)| < \varepsilon e^{-\alpha(t-T_{\varepsilon_1})} < \varepsilon$, $\forall t \in [T_{\varepsilon_1}, \bar{T})$. Then by the extension theorem of ODE, there is some small $\tau > 0$ such that the solution is defined in the $[T_{\varepsilon_1}, \bar{T} + \tau)$ and $|x^{NN}(t)| \leq \varepsilon e^{-\alpha(t-T_{\varepsilon_1})} < \varepsilon$, $\forall t \in [T_{\varepsilon_1}, \bar{T} + \tau)$. That is a contradiction by the definition of I .

4. In summary, let C be fixed constant in (A.4) larger than 2, and let ε be a constant in $(0, \gamma_0)$ sufficiently small. For $0 < \varepsilon_1 < \varepsilon/C < \gamma_0$ and

$$\delta < C^{-1}\beta e^{-CLT_{\varepsilon_1}\varepsilon_1}/2,$$

we have that

$$|x^{NN}(t) - x(t)| \leq \varepsilon, \quad \forall t \in (0, \infty),$$

and

$$|x^{NN}(t)| < \varepsilon e^{-\alpha(t-T_{\varepsilon_1})}, \quad \forall t \in (T_{\varepsilon_1}, \infty).$$

This yields the first conclusion.

5. Further, we have $|q(x^{NN}) - q(x)| \leq 2|Q||x^{NN} - x| \leq C|x^{NN} - x|$, and

$$\begin{aligned}
& |u^{NN}(x^{NN}) - u(x)| && \text{(A.5)} \\
& \leq |W^{-1}|[|g(x^{NN}) - g(x)||p^{NN}(x^{NN})| + \\
& \quad |g(x)||p^{NN}(x^{NN}) - p(x^{NN})| + |g(x)||p(x^{NN}) - p(x)|] \\
& \leq C(|x^{NN} - x| + \delta),
\end{aligned}$$

where $C > 0$ is a constant depending only on g, p, W . Hence by Theorem 3.2, for $\delta > 0$ sufficiently small, it holds that for some $\varepsilon < \gamma_0$,

$$|J(x^{NN}, u^{NN}) - J(x, u)| \leq C_2\varepsilon,$$

where C_2 is a constant depending only on f, g, R, p, W . This completes the proof. \square

ACKNOWLEDGEMENTS

The author is greatly indebted to Prof. Wei Kang for many helpful discussions and suggestions. The author would like to express his appreciation to Prof. Qi Gong and Dr. Tenavi Nakamura-Zimmerer for the useful suggestions and comments on the paper. Moreover, the author deeply thanks the anonymous referees for their insightful comments and suggestions which essentially improve the quality of this paper.

REFERENCES

- [1] R. W. Beard, G. N. Saridis, and J. T. Wen. Galerkin approximations of the generalized Hamilton–Jacobi–Bellman equation. *Automatica*, 33(12):2159–2177, 1997.
- [2] D. J Block, K. J Åström, and M. W Spong. The reaction wheel pendulum. *Synthesis Lectures on Control and mechatronics*, 1(1):1–105, 2007.
- [3] S. Cacace, E. Cristiani, M. Falcone, and A. Picarelli. A patchy dynamic programming scheme for a class of Hamilton–Jacobi–Bellman equations. *SIAM Journal on Scientific Computing*, 34(5):A2625–A2649, 2012.
- [4] P. Cannarsa and W. Cheng. Singularities of Solutions of Hamilton–Jacobi Equations. *Milan Journal of Mathematics*, 89(1):187–215, 2021.
- [5] G. Chen and G. Zhu. Symplectic algorithms for stable manifolds in control theory. *IEEE Transactions on Automatic Control*, 67(6), 3105–3111, 2022.
- [6] C. Cicone. *Ordinary differential equations with applications*, volume 34. Springer Science & Business Media, 2006.
- [7] Y. T. Chow, J. Darbon, S. Osher, and W. Yin. Algorithm for overcoming the curse of dimensionality for state-dependent Hamilton–Jacobi equations. *Journal of Computational Physics*, 387:376–409, 2019.
- [8] K. Chrysafinos and D. Plaka. Analysis and approximations of an optimal control problem for the Allen–Cahn equation. *Numer. Math.*, 155: 35–82, 2023.
- [9] P. Colli and J. Sprekels. Optimal control of an Allen–Cahn equation with singular potentials and dynamic boundary condition. *SIAM Journal on Control and Optimization*, 53(1):213–234, 2015.
- [10] J. Darbon and S. Osher. Algorithms for overcoming the curse of dimensionality for certain Hamilton–Jacobi equations arising in control theory and elsewhere. *Research in the Mathematical Sciences*, 3(1):19, 2016.
- [11] Q. Du and X. Feng. The phase field method for geometric moving interfaces and their numerical approximations. *Handbook of numerical analysis*, 21: 425–508, 2020.
- [12] W. E, J. Han, A. Jentzen. Algorithms for solving high dimensional PDEs: from nonlinear Monte Carlo to machine learning. *Nonlinearity*, 35(1):278, 2021.
- [13] J. Han, A. Jentzen, and W. E. Solving high-dimensional partial differential equations using deep learning. *Proceedings of the National Academy of Sciences*, 115(34):8505–8510, 2018.
- [14] S. Hochreiter and J. Schmidhuber. Long short-term memory. *Neural computation*, 9(8):1735–1780, 1997.
- [15] T. Horibe and N. Sakamoto. Nonlinear optimal control for swing up and stabilization of the acrobot via stable manifold approach: Theory and experiment. *IEEE Transactions on Control Systems Technology*, 27(6):2374–2387, 2019.
- [16] T. Horibe and N. Sakamoto. Optimal swing up and stabilization control for inverted pendulum via stable manifold method. *IEEE Transactions on Control Systems Technology*, 26(2):708–715, 2017.

- [17] K. Hornik. Approximation capabilities of multilayer feedforward networks *Neural networks*, 4(2):251–257, 1991.
- [18] F. Jiang, G. Chou, M. Chen, and C. J Tomlin. Using neural networks to compute approximate and guaranteed feasible Hamilton-Jacobi-Bellman PDE solutions. *arXiv preprint arXiv:1611.03158*, 2016.
- [19] E. Jones, T. Oliphant, P. Peterson, et al. Scipy: Open source scientific tools for python. 2001.
- [20] D. Kalise and K. Kunisch. Polynomial approximation of high-dimensional Hamilton–Jacobi–Bellman equations and applications to feedback control of semilinear parabolic pdes. *SIAM Journal on Scientific Computing*, 40(2):A629–A652, 2018.
- [21] W. Kang, Q. Gong, T. Nakamura-Zimmerer, and F. Fahroo, Algorithms of data development for deep learning and feedback design: A survey *Physica D: Nonlinear Phenomena*, 425: 132955, 2021.
- [22] W. Kang and L. Wilcox. A causality free computational method for HJB equations with application to rigid body satellites. In *AIAA Guidance, Navigation, and Control Conference*, page 2009, 2015.
- [23] W. Kang and L. C Wilcox. Mitigating the curse of dimensionality: sparse grid characteristics method for optimal feedback control and HJB equations. *Computational Optimization and Applications*, 68(2):289–315, 2017.
- [24] W. Kang and L. C Wilcox. Solving 1d conservation laws using Pontryagin Minimum Principle. *Journal of Scientific Computing*, 71(1):144–165, 2017.
- [25] K. Kunisch and D. Walter. Semiglobal optimal feedback stabilization of autonomous systems via deep neural network approximation. *ESAIM: Control, Optimisation and Calculus of Variations*, Vol. 27, artical number 16, 2021.
- [26] W. M. McEneaney. A curse-of-dimensionality-free numerical method for solution of certain HJB PDEs. *SIAM Journal on Control and Optimization*, 46(4):1239–1276, 2007.
- [27] T. Nakamura-Zimmerer, Q. Gong, and W. Kang. Adaptive deep learning for high dimensional Hamilton-Jacobi-Bellman equations. *SIAM Journal on Scientific Computing*, Vol. 43(2):A1221–A1247, 2021.
- [28] T. Nakamura-Zimmerer, Q. Gong, and W. Kang. Neural network optimal feedback control with guaranteed local stability. *IEEE Open Journal of Control Systems*, Vol. 1: 210–222, 2022.
- [29] T. Ohtsuka. Solutions to the Hamilton-Jacobi equation with algebraic gradients. *IEEE Transactions on Automatic Control*, 56(8):1874–1885, 2010.
- [30] D. Onken, L. Nurbekyan, X. Li, S. Fung, S. Osher, and L. Ruthotto. A neural network approach for high-dimensional optimal control applied to multiagent path finding. *IEEE Transactions on Control Systems Technology*, 31(1):1–17, 2022.
- [31] T. Poggio, H. Mhaskar, L. Rosasco, B. Miranda and Q. Liao. Why and when can deep-but not shallow-networks avoid the curse of dimensionality: a review. *International Journal of Automation and Computing*, 14(5):503–519, 2017.
- [32] M. Raissi. Forward-backward stochastic neural networks: Deep learning of high-dimensional partial differential equations. *arXiv preprint arXiv:1804.07010*, 2018.
- [33] I. M. Ross, Q. Gong, and P. Sekhavat. Low-thrust, high-accuracy trajectory optimization. *Journal of Guidance, Control, and Dynamics*, 30(4):921–933, 2007.
- [34] I.M. Ross, Q. Gong, M. Karpenko, and R.J. Proulx. Scaling and balancing for high-performance computation of optimal controls. *Journal of Guidance, Control, and Dynamics*, 41(10):2086–2097, 2018.
- [35] N. Sakamoto. Case studies on the application of the stable manifold approach for nonlinear optimal control design. *Automatica*, 49(2):568–576, 2013.
- [36] N. Sakamoto and A. J van der Schaft. Analytical approximation methods for the stabilizing solution of the Hamilton–Jacobi equation. *IEEE Transactions on Automatic Control*, 53(10):2335–2350, 2008.
- [37] J. Sirignano and K. Spiliopoulos. DGM: A deep learning algorithm for solving partial differential equations. *Journal of Computational Physics*, 375:1339–1364, 2018.
- [38] A. J. van der Schaft. On a state space approach to nonlinear H_∞ control. *Systems & Control Letters*, 16(1):1–8, 1991.
- [39] I. Yegorov and P. M. Dower. Perspectives on characteristics based curse-of-dimensionality-free numerical approaches for solving Hamilton–Jacobi equations. *Applied Mathematics & Optimization*, pages 1–49, 2018.

SCHOOL OF DATA SCIENCES, ZHEJIANG UNIVERSITY OF FINANCE & ECONOMICS, HANGZHOU
310018, ZHEJIANG, P. R. CHINA
Email address: `gychen@zufe.edu.cn`